

# Structural Properties of 1-Alkyl-3-methylimidazolium Bis{(trifluoromethyl)sulfonyl}amide Ionic Liquids: X-ray Diffraction Data and Molecular Dynamics Simulations

Enrico Bodo,<sup>\*,†</sup> Lorenzo Gontrani,<sup>‡</sup> Ruggero Caminiti,<sup>†</sup> Natalia V. Plechkova,<sup>§</sup> Kenneth R. Seddon,<sup>§,||</sup> and Alessandro Triolo<sup>⊥</sup>

Department of Chemistry and CNISM, University of Rome "Sapienza", Italy, P. A. Moro 5, 00185, Rome, Italy, Department of Chemistry, University of Rome "Sapienza", Italy, QUILL, The Queen's University of Belfast, Belfast BT9 5AG, Northern Ireland U.K., and CNR-Istituto di Struttura della Materia, Area della Ricerca di Roma 2, Tor Vergata, Rome, Italy

Received: September 29, 2010; Revised Manuscript Received: November 5, 2010

X-ray diffraction data for 1-alkyl-3-methylimidazolium bis{(trifluoromethyl)sulfonyl}amides are reported as a function of the length of the alkyl chain on the imidazolium ring. The measured diffraction patterns have been compared with the theoretical patterns calculated (from the geometries obtained) with molecular dynamics simulations. This provides a detailed description (at the atomistic level) of the morphology in the liquid state of these salts, highlighting the role played by the alkyl chain length. An analysis of the behavior of the hydrogen bonds that are formed between the imidazolium acidic protons and the anion is presented.

## Introduction

Ionic liquids<sup>1–3</sup> with low volatilities and low melting points have represented, in the last ten years, a rich field of research because of their many applications in diverse technological research areas.<sup>4</sup> These substances contain both a cation (which can, for example, be an asymmetric derivative of the 1-alkylpyridinium, tetraalkylphosphonium, 1,3-dialkylimidazolium, or tetraalkylammonium ions) and an anion, which can be as simple as chloride or a more complex structure such as bis{(trifluoromethyl)sulfonyl}amide [NTf<sub>2</sub>]<sup>−</sup>. Their versatility depends on the fact that their properties can be tuned by varying the cation and the anion.

Together with the very large number of experimental studies of ionic liquids,<sup>5–8</sup> molecular simulations based on classical force fields have played a crucial role in providing the link between the physical and chemical properties and the molecular structure at the nanoscopic level.<sup>9</sup> Since their introduction to the scientific community,<sup>10</sup> the force fields for molecular dynamics (MD) simulations of ionic liquids have been refined, expanded<sup>11,12</sup> and reparametrized several times (see, for example, ref 13 and references therein) and have now reached a point in which molecular dynamics simulations are able to make reliable predictions of many liquid properties. For example, we have recently used such force fields to provide an interpretation of the first X-ray diffraction studies of the [C<sub>n</sub>mim] Br (where [C<sub>n</sub>mim]<sup>+</sup> = 1-alkyl-3-methylimidazolium, alkyl = C<sub>n</sub>H<sub>2n+1</sub>, 1 < n < 18) ionic liquid.<sup>14</sup>

The bis{(trifluoromethyl)sulfonyl}amide anion was first introduced into the ionic liquid literature in 1996 as a basis for hydrophobic electrolytes for electrochemical studies.<sup>15</sup> Its air and water stability combined with its lack of chemical reactivity have made it a popular ion for experimental and theoretical studies to the extent that a IUPAC committee selected a 1-hexyl-

3-methylimidazolium bis{(trifluoromethyl)sulfonyl}amide ([C<sub>6</sub>mim]-[NTf<sub>2</sub>]) as a standard for comparing the variability of experimental measurements carried out by different research groups.<sup>16,17</sup> In 2004, Canongia Lopes and Pádua<sup>18</sup> proposed an optimized potential for liquid simulations (OPLS-AA) derived force field for the description of the anion that has proven to provide reliable quantities when compared to experimental observables.

Earlier density measurements for these compounds date back to 1996.<sup>15</sup> Various studies have then expanded the set of measured observables and provided their dependence both on temperature and in the homologous series of these compounds obtained by varying the length of the alkyl chain on the imidazolium cation. A list of the known properties for the title ionic liquids is reported in Table 1.

It was found by Watanabe et al.<sup>26</sup> that, in the series of [C<sub>n</sub>mim][NTf<sub>2</sub>] ionic liquids, the viscosity increases with increasing n together with the self-diffusion coefficient. To explain such counterintuitive experimental data, Urahata and Ribeiro<sup>27</sup> and Wang and Voth<sup>28</sup> carried out united-atom and coarse grained theoretical simulations of imidazolium based ionic liquids concluding that the apolar, nearly neutral alkyl chains tend to self-assemble. When the size of the chains is large enough, both MD simulations and experiments highlighted that this segregation effect leaves a clear imprint in the diffraction patterns and in the radial distributions functions (RDF).<sup>25,29,30</sup> Hardacre and co-workers<sup>31</sup> explored the structure of the [C<sub>1</sub>mim][NTf<sub>2</sub>] by neutron diffraction and theoretical simulations, concluding that the liquid phase had peculiar geometric features: for example, the anion was found to be predominantly in the trans orientation, whereas the solid phase is known to have a cis preference; moreover, as opposed to [C<sub>1</sub>mim]Cl or [C<sub>1</sub>mim][PF<sub>6</sub>], [C<sub>1</sub>mim][NTf<sub>2</sub>] is found to show negligible long-range alternating counterion ordering. More generally, as opposed to the other mentioned ionic liquids, this material is characterized by a liquid structure that shows only limited resemblance to the layered crystalline one. A reason for such contrasting structures might be the high flexibility of the [NTf<sub>2</sub>]<sup>−</sup> anion, which can be thermally activated in the liquid state. Other geometrical features of these ionic liquids, such as

\* To whom correspondence should be addressed. E-mail: bodo@caspur.it.

<sup>†</sup> Department of Chemistry and CNISM, University of Rome "Sapienza".

<sup>‡</sup> Department of Chemistry, University of Rome "Sapienza", Italy.

<sup>§</sup> QUILL, The Queen's University of Belfast.

<sup>||</sup> Universidade Nova de Lisboa.

<sup>⊥</sup> CNR-Istituto di Struttura della Materia.

**TABLE 1: Measured Properties of [C<sub>n</sub>mim][NTf<sub>2</sub>]**

side chain length <i>n</i>	property	reference
1–3	density, melting point, viscosity, refractive index, thermal stability	15
2–10	phase transition, density, viscosity, surface tension	19
2–3	density, melting temperatures, phase transition, thermal stability, heat capacity	20
1–3, 6, 8	density, viscosity, diffusion coeff., ionic conductivity	21
3	phase transition, density, refractive index, surface tension, solvatochromic effect	22
1–10	small/large angle X-ray scattering	23–25

the relative conformations of the side alkyl chains, were also analyzed and reported previously.<sup>12</sup> Canongia Lopes and Pádua<sup>32</sup> in 2006 investigated the above-mentioned side chain segregation effects in [C<sub>n</sub>mim][NTf<sub>2</sub>] ionic liquid and showed the presence of a network of polar domains (composed of the charged heads of imidazolium cation and of the anions) and a “continuous microphase” of nonpolar domains made by the alkyl chains when *n* > 2, and attributed to the experimental viscosity behavior to the presence of these microdomains. While the force field model of Canongia Lopes and co-workers<sup>18</sup> was able to provide a robust theoretical framework for this kind of topological model, it failed in reproducing other physicochemical properties such as heats of vaporization. From reparametrization of the force field in ref 33 where the authors provided a new set of Lennard-Jones parameters, the accuracy in the prediction of several properties, especially densities and enthalpies of vaporization, improved significantly.<sup>34</sup> More recently, a theoretical study<sup>35</sup> has provided ab initio optimized gas-phase structures of several ion pairs in [C<sub>n</sub>mim][NTf<sub>2</sub>] ionic liquids with *n* = 4, 6, or 8 and has shown that the size of the lateral alkyl chain has little effect on the RDF. Elsewhere,<sup>23</sup> X-ray diffraction data have been compared with MD simulations to unravel the geometric structure of the [C<sub>2</sub>mim][NTf<sub>2</sub>] ionic liquid and have shown the presence of a mixture of two anion conformers (see Figure 1). Recently, some of us reported a joined small angle X-ray scattering/Kerr effect spectroscopic study on a series of [C<sub>2</sub>mim][NTf<sub>2</sub>] salts (with 1 < *n* < 10) highlighting structural and dynamic features of this family of ionic liquids.<sup>24</sup> In particular, it was shown that only *n* > 3 alkyl chains tend to self-assemble into apolar domains. Joint Raman spectroscopic data and DFT calculations were applied to explore the conformational equilibrium of the anion in [C<sub>2</sub>mim][NTf<sub>2</sub>], suggesting a restricted rotation about the S–N bond leading to a facile interconversion between cis and trans conformers.<sup>37,38</sup>

Given the large number of studies on this class of ionic liquids, we undertook the first combined experimental and theoretical studies of X-ray diffraction structure factors and the

relative radial functions for a series of 1-alkyl-3-methylimidazolium bistriflamide salts, where *n* = 1, 4, 6, or 8. This study provided a detailed atomistic level description of the morphology of these salts in the liquid state, highlighting the role played by the alkyl chain length.

### Experimental Section

1-Alkyl-3-methylimidazolium bis{(trifluoromethyl)sulfonyl}amides (alkyl = butyl, hexyl, octyl) were purchased from Iolitec.<sup>39</sup> 1,3-Dimethylimidazolium bis{(trifluoromethyl)sulfonyl}amide was synthesized according to the following procedure: 1,3-Dimethylimidazolium methyl sulfate (30.85 g, 0.148 mol) and Li[NTf<sub>2</sub>] (43.39 g, 0.151 mol) were dissolved in water (250 cm<sup>3</sup>) and stirred for 10 h, during which the mixture separated into two phases. Dichloromethane (300 cm<sup>3</sup>) was added to this mixture. The upper aqueous phase was discarded and the lower dichloromethane layer was washed with water (6 × 200 cm<sup>3</sup>) and dried over anhydrous magnesium sulfate (20 g), which was then removed by filtration. The filtrate was heated in vacuo at 40 °C to remove the excess solvent. The product was obtained as a transparent paste (46.20 g, 0.122 mol, 81% yield). <sup>1</sup>H NMR spectra (300 MHz, trichloromethane-*d*<sub>1</sub>) showed chemical shifts δ 3.86 (s, 6H, NCH<sub>3</sub>), 7.31 (s, 2H, NCHCH), and 8.84 ppm (s, 1H, NCHN) and a melting point (DSC) of 23.35 °C.

The four samples, after drying for 24 h in vacuo at 60 °C, to reduce the moisture content, were rapidly put into a cell sealed with Mylar windows. Sample and windows thicknesses were 3 mm. The large angle X-ray scattering (LAXS) experiments were conducted at room temperature using the noncommercial energy-scanning diffractometer built in the Department of Chemistry, Rome University “Sapienza” (Italian Pat. Appl. no. 1126484 - 23 June 1993, Caminiti et al.)<sup>40,41</sup> White Bremsstrahlung radiation emitted by a tungsten tube (50 kV, 40 mA) was used. The expression for the scattering variable *s* (transferred momentum) is

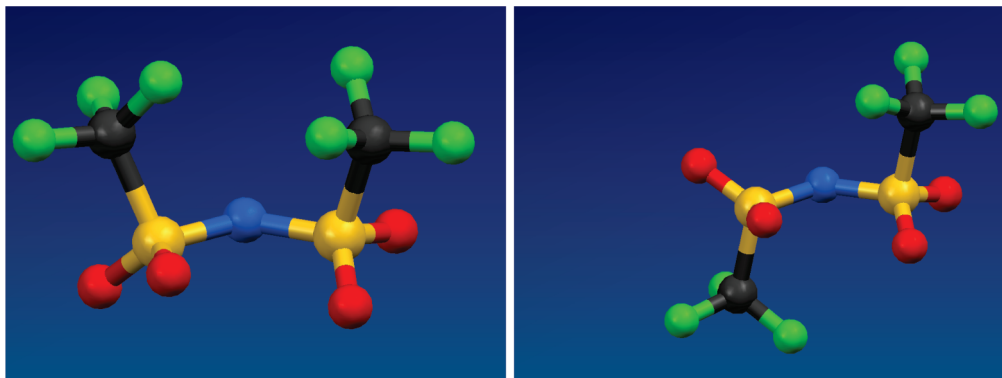


**Figure 1.** Cisoid (left) and transoid (right) isomers of the bistriflamide anion, [CF<sub>3</sub>SO<sub>2</sub>NSO<sub>2</sub>CF<sub>3</sub>]<sup>-</sup>. Both of these forms were identified crystallographically.<sup>37</sup> In solution there is a rapid interchange between these two.

$$s = \frac{4\pi \sin(\theta)}{\lambda} \approx E \cdot 1.014 \sin(\theta) \quad (1)$$

when  $E$  is expressed in keV and  $s$  in  $\text{\AA}^{-1}$ .

The primary beam intensity  $I_0(E)$  was measured directly, by reducing the tube current to 10 mA without the sample. Transmission of the sample was measured under the same conditions. Both quantities are needed to carry out the necessary absorption corrections to experimental data. The ultrathin Mylar cell windows contribution to the diffraction intensity is less than 1/10 000 of the total. After correction of experimental data for escape peak suppression,<sup>42</sup> the various angular data were normalized to a stoichiometric unit of volume containing one ion pair and merged to yield the total static structure factor,  $I(s)$ , in momentum-space.  $I(s)$  is equal to

$$I(s) = I_{\text{cu}} - \sum_{i=1}^n x_i f_i(s)^2 \quad (2)$$

where  $f_i(s)$  are the interpolated atomic scattering factors,<sup>43,44</sup>  $x_i$  are the number concentrations of  $i$ -type atoms in the stoichiometric unit, and  $I_{\text{cu}}$  is the observed intensity in electron units. The function was multiplied by  $sM(s)$  where  $M$  is an  $s$ -dependent sharpening factor defined in eq 3

$$M(s) = \frac{f_N^2(0)}{f_N^2(s)} \exp(-0.01s^2) \quad (3)$$

having chosen nitrogen as the sharpening atom. Fourier transformation of  $I(s)$  led to RDF in distance space,  $D(r)$ :

$$D(r) = 4\pi r^2 \rho_0 + \frac{2r}{\pi} \int_0^{s_{\text{max}}} s I(s) M(s) \sin(rs) ds \quad (4)$$

In this equation,  $\rho_0$  is the bulk number density of stoichiometric units. We used the value of  $19.56 \text{\AA}^{-3}$  (last experimental point) as the upper limit of integration. Subtraction of the  $4\pi r^2 \rho_0$  term (corresponding to a uniform distribution) from this formula allows the isolation of the structural contribution to the distribution function ( $Diff(r)$ ). The latter RDF is more suited to highlight intermolecular (medium-long-range) interactions than the more commonly used  $G(r)$ . Detailed description of procedures and formulas used can be found in refs 42, 45, and 46.

## Calculations

All-atom MD simulations have been carried out on pure  $[\text{C}_n\text{mim}][\text{NTf}_2]$  ionic liquids with  $n = 1, 4, 6,$  or  $8$  using the DLPOLY2<sup>47</sup> package. We have employed two force fields: the one from Canongia Lopes and Pádua<sup>11,18,48</sup> and the one from Köddermann et al.<sup>33</sup> The latter was used only for  $n = 4$  and  $6$ . A sketch of the template structures and the labels of the atoms used in the FF are displayed in Figure 2.

The initial configurations have been generated by randomly distributing 550 ionic couples in very large simulation cells. A short (100 ps) isobaric–isothermal ( $NPT$ ) run at 500 K and with  $10^3$  atmospheres pressure was carried out to provide densely packed, mixed initial configurations. These initial configurations were left to relax during another  $NPT$  run of 300–500 ps at 1 atm and 300 K up to the point in which an approximately constant density was obtained. The volume was then fixed and

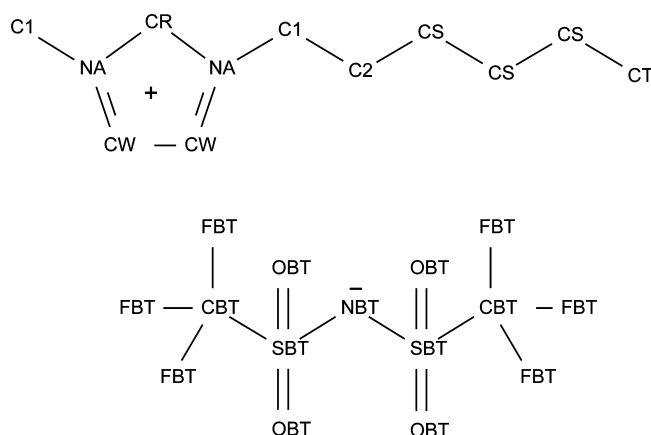


**Figure 2.** Sketch of the template structures and the labels of the atoms used in the FF.

**TABLE 2: Calculated and Measured Densities in  $\text{g cm}^{-3}$  for  $[\text{C}_n\text{mim}][\text{NTf}_2]^a$**

$n$	Canongia Lopes FF	Köddermann FF	expt
1	1.63		1.557
4	1.49	1.43	1.438
6	1.40	1.37	1.364
8	1.37		1.320

<sup>a</sup> Densities from ref 26.

an additional mixing was provided by a short (300 ps)  $NVT$  run at 300 K where the electrostatic interactions were turned off. The resulting configurations were finally left to evolve in a constant volume  $NVT$  production run of about 5 ns with  $T = 300$  K after an equilibration period. The theoretical densities are compared with the experimental ones in Table 2.

All the bonds involving the hydrogen atoms have been kept constrained using the Shake algorithm while no other degrees of freedom were restricted. The system was treated in a periodic box of around  $70^3 \text{\AA}^3$  containing 550 ionic couples. Nonbonded interactions were computed up to  $9 \text{\AA}$ . To test the quality of this choice, a few hundred additional picosecond runs with the cutoff value set to  $12.0 \text{\AA}$  were performed and we found that the results were largely insensitive to this choice. The long-range electrostatic interactions were accounted for by means of the smoothed particle mesh Ewald (SPME) solver with a precision of  $10^{-6}$ . The integration time step for the leapfrog algorithm was 1 fs in the production run and a snapshot of the configuration was saved each 20 ps to be used in the geometric analysis.

Each production run produced a few hundred snapshots that were then employed in the calculation of the structure function following the Debye scattering equations:<sup>49</sup>

$$I(s) = \sum_i \sum_j f_i(s) f_j(s) x_i x_j \frac{\sin(sr_{ij})}{sr_{ij}} \quad (5)$$

where  $f_i(s)$  and  $f_j(s)$  are the atomic scattering factors and  $x_i$  and  $x_j$  are the number concentrations of  $i$ - and  $j$ -type atoms in the stoichiometric unit. From  $I(s)$ , it is possible to extract the RDF  $Diff(r)$  by means of eq 4. It is important to point out that in the very low  $s$  range ( $s < 1.2 \text{\AA}^{-1}$ ) the theoretical  $I(s)$  is unreliable due both to the limited box size and to the Debye formula we have used. We therefore cut our simulated values at  $s \sim 1 \text{\AA}^{-1}$  and smoothly joined them with the experimental low  $s$  sets of data before performing the integration of eq 4.

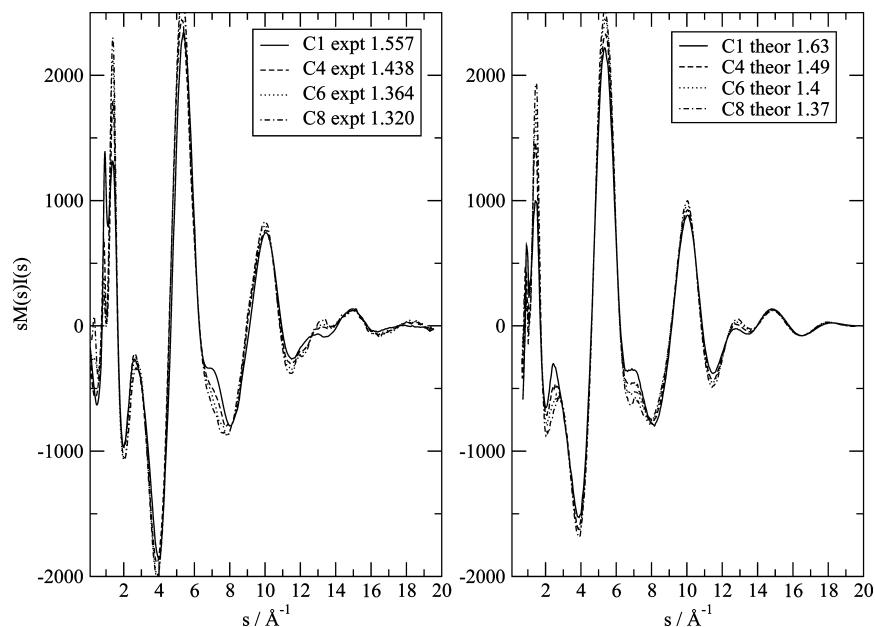


**Figure 3.**  $sM(s)I(s)$  for the four ionic liquids. Left: measured quantities. Right: simulated structure factors. The numbers in the captions are the densities in  $\text{g cm}^{-3}$ . The simulations reported here are obtained with Canongia Lopes force field.

## Results and Discussion

Table 2 reports the MD-computed densities compared with the experimentally determined values, as a validation of the simulation. The densities obtained with the Canongia Lopes force field are larger than the experimental ones, while those calculated with the Ködderman force field are in much better agreement.<sup>33</sup>

As shown in the Introduction, many key structural features of the present ionic liquids have already been described in the literature:

1. With a side chain longer than four carbon atoms, chain aggregation in nonpolar domains is visible in the experimental<sup>24</sup> as well as in the theoretical structure factor  $I(s)$  as low- $s$  distinctive peaks.<sup>28,32</sup> This aggregation effect may explain the behavior of experimental quantities such as viscosity, diffusion coefficients and ionic conductivity;<sup>32</sup>
2. In the anion, the trans conformation is dominant with respect to the cis<sup>31,37,38</sup> one (see Figure 1);
3. In the side chain, the conformation of the carbon–carbon dihedral angle becomes more and more sharply defined as one moves from the carbon near the ring to the end of the chain: the C–C dihedral angles are predominantly in the anti conformation;<sup>12</sup>
4. The length of the side chain has relatively little effect on the RDFs. The liquid local structure is due to the coexistence of various conformers that can be identified by in vacuo ab initio calculations.<sup>35</sup>
5. A comparison between LAXS experiments and MD simulations<sup>23</sup> has established a few important features of the liquid structure of [C<sub>2</sub>mim][NTf<sub>2</sub>]. In particular, it has been shown that the imidazolium ring carbon atoms are all mainly correlated with the oxygen atoms of the sulfonyl groups in the anion. The strongest interaction is attributed to the CR atom (see Figure 2). Whether this interaction has to be attributed to hydrogen bonding or not depends on the definition of hydrogen bonding, which is rather fuzzy.<sup>50,51</sup>

The experimental (left) and theoretical (right) structure factors, as measured and calculated by eq 5, are illustrated in Figure 3. The theoretical data reported here were obtained using the

Canongia Lopes force field and are in fairly good agreement with the experiments: they reproduce both the intensity and positions of most of the experimental peaks.

In particular, the peaks at 6 and 10  $\text{\AA}^{-1}$  are accurately duplicated, as is the shoulder between 6.5 and 8  $\text{\AA}^{-1}$ . These are due to structural correlations in the intramolecular range. Below 4  $\text{\AA}^{-1}$  the agreement between the theory and the experiment deteriorates but it is still possible to match all the peaks positions although not their intensities. The total  $I(s)$  has been presented in ref 23 for the [C<sub>2</sub>mim][NTf<sub>2</sub>] liquid. By visual comparison of Figure 3 with Figure 2 of ref 23, [C<sub>1</sub>mim][NTf<sub>2</sub>] and [C<sub>2</sub>mim][NTf<sub>2</sub>] can be seen to present a similar profile in which the first two peaks (those centered at ca. 0.9 and 1.5  $\text{\AA}^{-1}$ ) have similar heights, while for [C<sub>*n*</sub>mim][NTf<sub>2</sub>] ( $n \geq 4$ ) the peak at 0.9  $\text{\AA}^{-1}$  is weaker. The low- $s$  region of Figure 3 is reported in Figure 4 with an expanded  $s$ -scale. These experimental data are in very good agreement with those reported in ref 24. In the low- $s$  region, we see three distinct peaks: 2.6–2.8, 1.4, and 0.8  $\text{\AA}^{-1}$ . These peaks are due to structures in the range 2–8  $\text{\AA}$  in the direct space. As can be seen, the force fields and the simulations are accurate enough to reproduce the 2.6–2.8  $\text{\AA}$  peak, though the different ionic liquids show a somewhat more marked difference in the simulated data than in the experimental counterpart. The second peak at 1.4  $\text{\AA}^{-1}$  is well reproduced by the simulation, which accounts correctly for the different intensities of the various ionic liquids. Since this peak is due to structures around 5  $\text{\AA}$ , it is a good test of the reliability of the employed force fields in reproducing the structural correlations. The intensity of this peak is proportional to the length of the side chain and, therefore, can be probably attributed to the characteristic 5  $\text{\AA}$  feature that can be seen in the RDFs already reported by other authors (see refs 28 and 32) and that has been attributed to the side chain aggregation effect.<sup>27,29</sup>

At around 1  $\text{\AA}^{-1}$ , there is a third low- $s$  peak that should point out the presence of long-range structuring. This structure is more prominent for the shortest chain, [C<sub>1</sub>mim][NTf<sub>2</sub>]. Unfortunately, in the simulation of [C<sub>1</sub>mim][NTf<sub>2</sub>], this feature, though present, is not as prominent as in the experimental profile and this prevented a clear identification of a geometric feature explaining such a result.

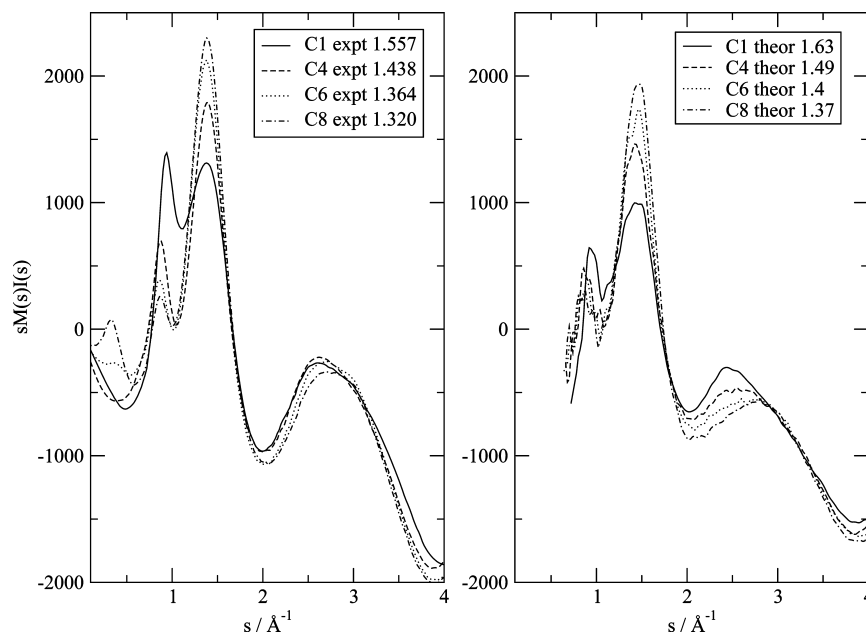


**Figure 4.**  $sM(s)I(s)$  for the four ionic liquids,  $[C_n\text{mim}][\text{NTf}_2]$  (where  $n = 1, 4, 6,$  or  $8$ ). Left: measured quantities. Right: simulated structure factors. The numbers in the captions are the densities in  $\text{g cm}^{-3}$ . The simulations reported here are obtained with the Canongia Lopes force field.

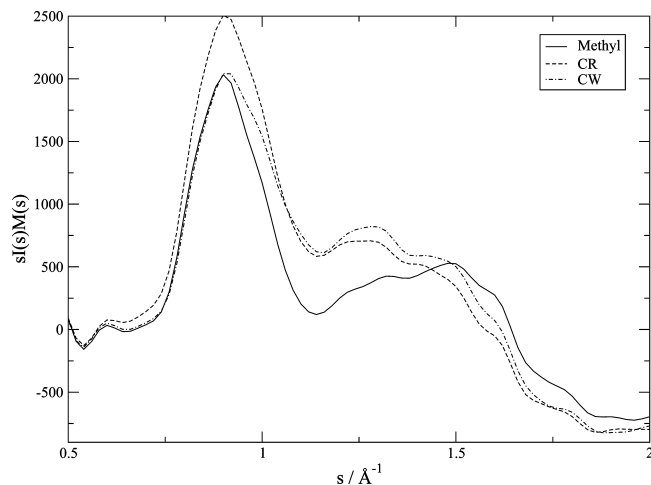


**Figure 5.**  $I(s)$  calculated by activating the contribution of the carbon/hydrogen groups indicated in the legend. (See Figure 2 for notation.)

To investigate the presence of this peak, we have calculated the static structure factors setting to zero the scattering factors of some carbon/hydrogen atoms in the imidazolium ring, while leaving the others unchanged. In particular, Figure 5 illustrates the structure factors obtained by activating the contribution of one of the C1/H1, CW/HCW, and CR/HCR groups and setting to zero the other two. As evident from Figure 5, the exclusion of C1/H1 and CW/HCW groups in the calculation (i.e., only CR/HCR is active among the carbon ring atoms) makes the peak considerably more pronounced than in the case where methyl and CW-HCW groups are activated. The role played by CR/HCR in the intermolecular interactions complies with the structural pattern that has been found in crystalline  $[C_1\text{mim}][\text{PF}_6]$ ,<sup>36</sup> where each HCR interacts with two  $\text{PF}_6$  anions, and suggests that a certain degree of local order might be preserved in liquid  $[C_1\text{mim}][\text{NTf}_2]$ .

Starting with  $[C_8\text{mim}][\text{NTf}_2]$ , a prepeak located at  $0.3 \text{ \AA}^{-1}$  appears, which can be observed also for  $[C_6\text{mim}][\text{NTf}_2]$ , albeit with more difficulty; but it is absent for shorter chain lengths. The distances involved in that signal are around  $25 \text{ \AA}$ . Theoretical studies of these long-range ordering effects in

imidazolium based ionic liquids have been carried out in the aforementioned papers by Urahata and Ribeiro,<sup>27</sup> Wand and Voth,<sup>28</sup> and by Canongia Lopes and Pádua.<sup>32</sup> Experimental work on these low- $s$  features and a more detailed discussion on their nature can be found in the work by Triolo et al.<sup>29</sup>

Some of the above calculations, namely for the  $[C_4\text{mim}][\text{NTf}_2]$  and  $[C_6\text{mim}][\text{NTf}_2]$  systems, have been repeated with the more recent force fields by Köddermann et al. and produced better densities.<sup>33</sup> The  $sM(s)I(s)$  calculated with the latter force field are reported in Figure 6. As can be seen, above  $3 \text{ \AA}^{-1}$  (below  $2 \text{ \AA}$ ) the Köddermann and Canongia Lopes force fields provide substantially the same results and this is a rather obvious result since the intramolecular part of the force field is the same. The two force fields show small differences at long range, i.e., below  $3 \text{ \AA}^{-1}$ , but it is hard to say which one scores better in predicting the peak positions, while for both the agreement on the intensities remains uncertain.

From the  $I(s)$ , the total radial distribution function or, to better visualize the various contributions, the  $\text{Diff}(r)$  of eq 4 can be easily obtained. Figure 7 represents the  $\text{Diff}(r)$  for the four ionic liquids compared with those coming from the Fourier transform of the experimental structure factors. For all the ionic liquids the results were obtained from the calculations performed with the Canongia Lopes force field, while for  $[C_4\text{mim}][\text{NTf}_2]$  and  $[C_6\text{mim}][\text{NTf}_2]$  the results are also presented for the Köddermann one. Again, the intramolecular radial distribution function, i.e., the spectral range below  $3 \text{ \AA}$  has been accurately reproduced. The Canongia Lopes force field, however, seems to perform better at long-range, especially in reproducing the amplitudes of the oscillations between  $5$  and  $15 \text{ \AA}$ . In general, both force fields are quantitatively in good agreement with the experimental data and describe correctly the shape of the long-range RDF in the longer side chain compounds.

The experimental result (Figure 7 black circles) clearly indicates a substantial difference between  $[C_1\text{mim}][\text{NTf}_2]$  and  $[C_n\text{mim}][\text{NTf}_2]$  ( $n > 1$ ). Pronounced oscillations are, in fact, clearly visible on the long-range scale while they are suppressed for  $[C_6\text{mim}][\text{NTf}_2]$  and  $[C_8\text{mim}][\text{NTf}_2]$ . Unfortunately the results reported in Figure 5 of ref 23 are limited to distances below  $20$

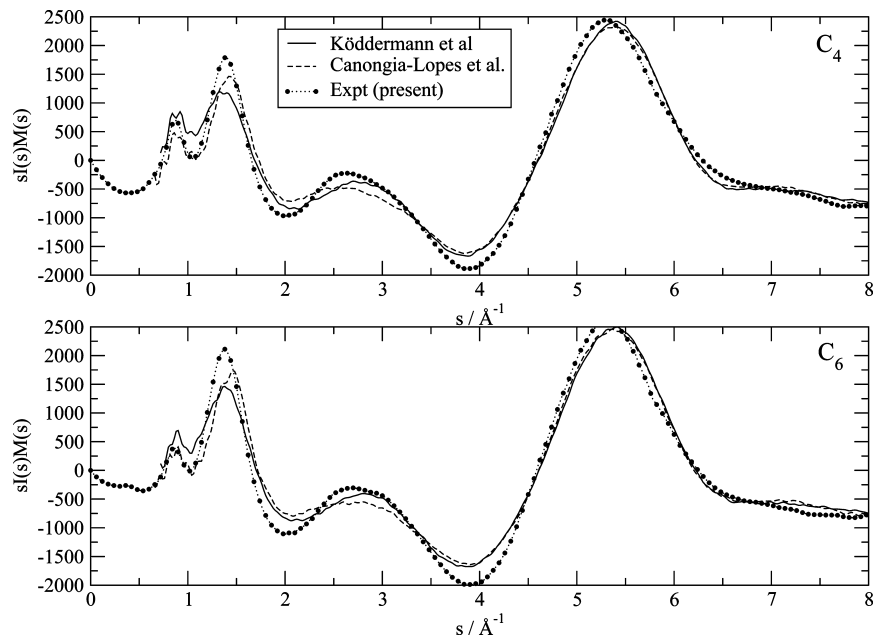


Figure 6.  $sI(s)M(s)$  for the [C<sub>4</sub>mim] (above) and [C<sub>6</sub>mim] (below) ionic liquids with two force fields compared to the experimental determination.

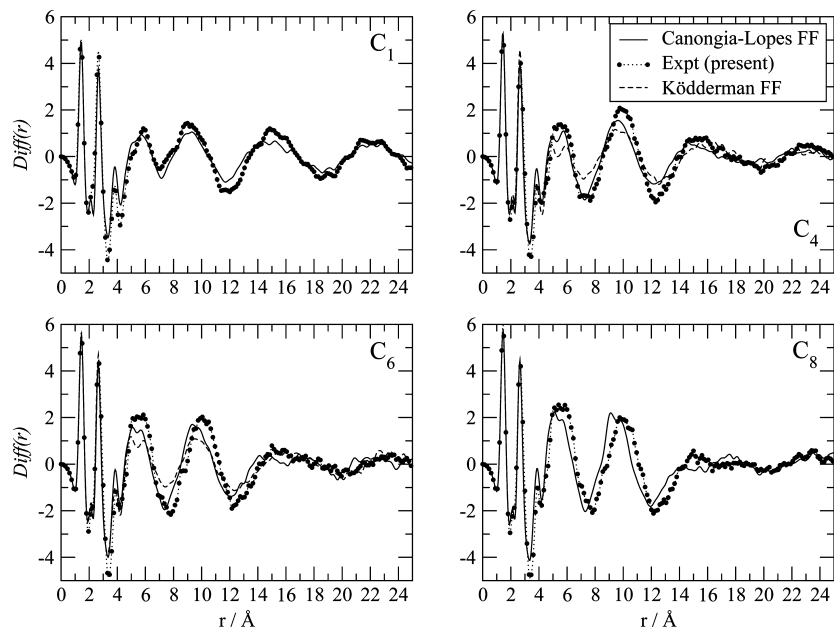


Figure 7.  $Diff(r)$  for [C<sub>n</sub>mim][NTf<sub>2</sub>] with  $n = 1$  (upper-left corner),  $n = 4$  (upper-right),  $n = 6$  (lower-left),  $n = 8$  (lower right). Both experimental and theoretical data are reported (two force fields where available).

Å and it is difficult to say whether [C<sub>2</sub>mim][NTf<sub>2</sub>] shows long-range structuring effects as for the [C<sub>1</sub>mim][NTf<sub>2</sub>].

It is possible to assign most of the short-range peaks using our simulation: the first peak is due to a coalescence of C–F, S–O, and S–N pair distributions in the [NTf<sub>2</sub>]<sup>-</sup> anion and to C–C distributions in the imidazolium cation. The small second peak at 2.1–2.2 Å is mainly due to F···F pairs in the anion and to C–C interactions in the imidazolium ring. The third feature between 2.5 and 3.0 Å is due to various pair contributions in the anion superimposed on those coming from alkyl chains of the cation. The peak at 4 Å is due to F···N and F···O contributions. The anion–cation intermolecular contributions form an almost continuous background starting at 3 Å and this is what we see in the  $Diff(r)$  between 4.5 and 7 Å. In Figure 8, these findings are summarized for the special case of [C<sub>6</sub>mim][NTf<sub>2</sub>].

The relative conformation of the anion has already been shown to be predominantly of trans type.<sup>31</sup> It is very simple to provide a further confirmation of this aspect of the local geometric structure by looking at the CBT–CBT RDFs (see Figure 2 and Figure 9). It can be seen that the second peak (corresponding to the larger C–C distance) is always dominant in our simulations. Unfortunately, in the experimental data, this information is hidden in the  $Diff(r)$  because it is superimposed onto the peaks coming from the intermolecular interactions.

The local structure of the anion can be also characterized by the analysis of its torsional angles.<sup>12,35</sup> The probability distribution of the dihedral angles for two representative choices of the atoms in the chain: the S–N–S–C angle and the O–S···S–O angle are shown in Figure 10. The former distribution is rather broad and slightly irregular. It is in agreement with that shown in ref 35 and clearly denotes the existence of two conformers,

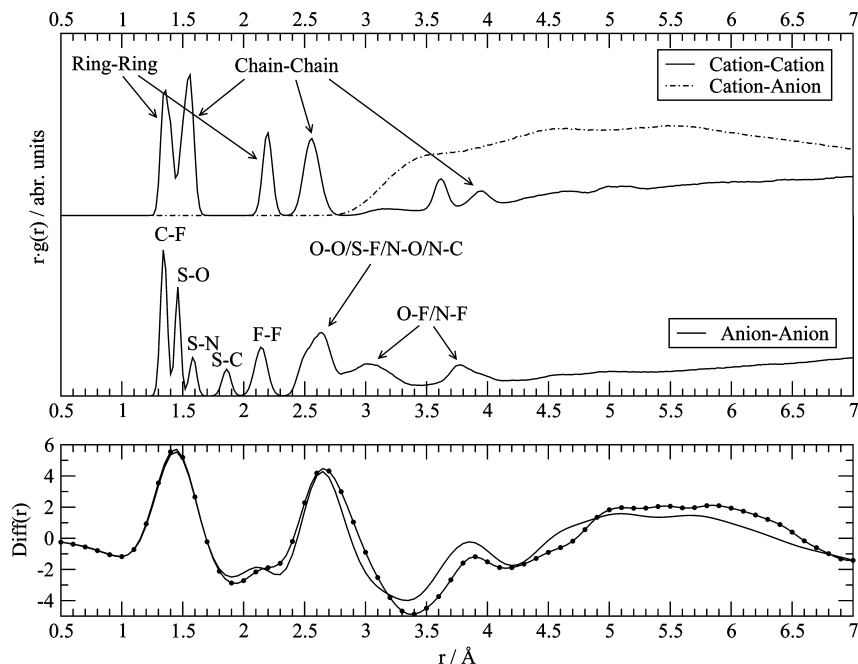


**Figure 8.** Lower panel: experimental (circles) and theoretical (line)  $Diff(r)$  for  $[C_6mim][NTf_2]$ . Upper panel: selected RDFs for various intra- and intermolecular pairs.

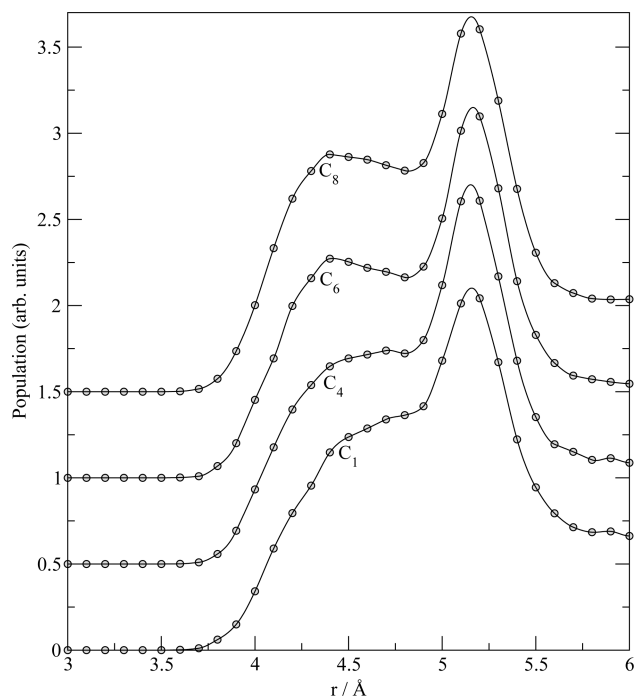


**Figure 9.** C–C RDF in the  $[NTf_2]^-$  anion for the four ionic liquids analyzed here.

one with dihedral angles around 90 and 270° and another with the angles around 120 and 240°. The first conformer is the most stable<sup>12</sup> and also the most populated. The O–S···S–O angles show instead that the highly polarized oxygen atoms in the anion clearly prefer an anti conformation. It is notable that the structure of the anion depends very little on the size of the alkyl chain on imidazolium.

The conformation of the alkyl side chain on imidazolium can be characterized by an analogous analysis of the dihedral angles between carbon atoms. The probability distribution for such angles is shown in Figure 11. In each of three columns, the results for  $[C_4mim][NTf_2]$ ,  $[C_6mim][NTf_2]$ , and  $[C_8mim][NTf_2]$

are described. In the first row, the probability distribution for the angle formed by the first two carbon atoms with respect to the CR–NA direction is reported. The distribution is rather broad although it shows a certain preference for the torsional energy minima,<sup>12</sup> thus confirming that for side chains longer than ethyl, there is a considerable freedom of rotation around the NA–C1 bond. The second row reports the dihedral for the NA–C1–C2–CS sequence. The anti and gauche conformers that are known to have a comparable energy clearly predominate.<sup>12</sup> It is interesting to note that the rotational mobility around the C1–C2 bond is drastically reduced with respect to that around the NA–C1 bond. As the chain gets longer, it behaves as in liquid hydrocarbons, and all its torsional angles prefer the anti conformation with little preference for the gauche (see the third row of Figure 11). We conclude that in these liquids, the alkyl chain is relatively free to rotate around its very first connections to the ring while its relative conformation becomes more rigid the further from the ring the carbon atoms reside.

The hydrogen atoms on the imidazolium ring are slightly acidic<sup>51,52</sup> and can partake in a special form of hydrogen bond with the negatively charged atoms of the anion. Figure 12 shows an analysis of the RDF of the two kind of hydrogen atoms on the imidazolium ring and the various negatively charged terminal atoms of the anion. Although both the nitrogen and the fluorine atoms do present some correlation with the protons, it is evident that the hydrogen bond is formed with the oxygen of the sulfonyl groups. Despite having a larger partial charge than oxygen, the nitrogen seems unable to form a stable “hydrogen bond” with the imidazolium ring, probably because of the repulsive steric effect due to the presence of the two sulfonyl groups. The “hydrogen bond” with the HCR atom (which is also the most acidic) is the strongest and leads to a distinctive feature in the RDF at 2.5 Å. The situation for the other three ionic liquids is quite similar and is illustrated by Figure 13. The strength of the hydrogen bonding is larger for the HCR atom and increases slightly with the size of the alkyl chain. In the same Figure, the RDF for the CR–OBT distance (compared with those reported in Figure 6 of ref 23) are shown, and hence we can easily

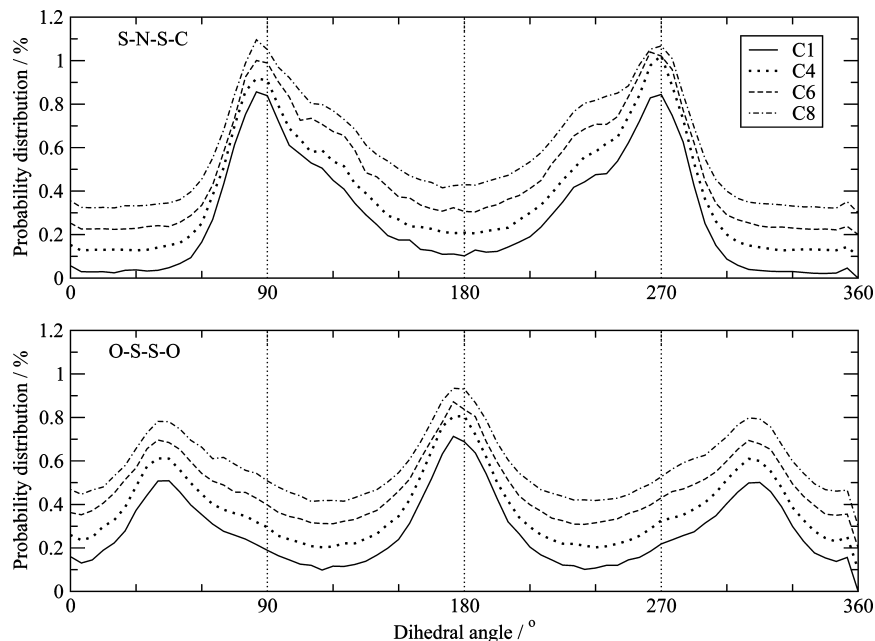


**Figure 10.** Dihedral angles probability distribution for the [NTf<sub>2</sub>]<sup>-</sup> anion for the four ionic liquids.

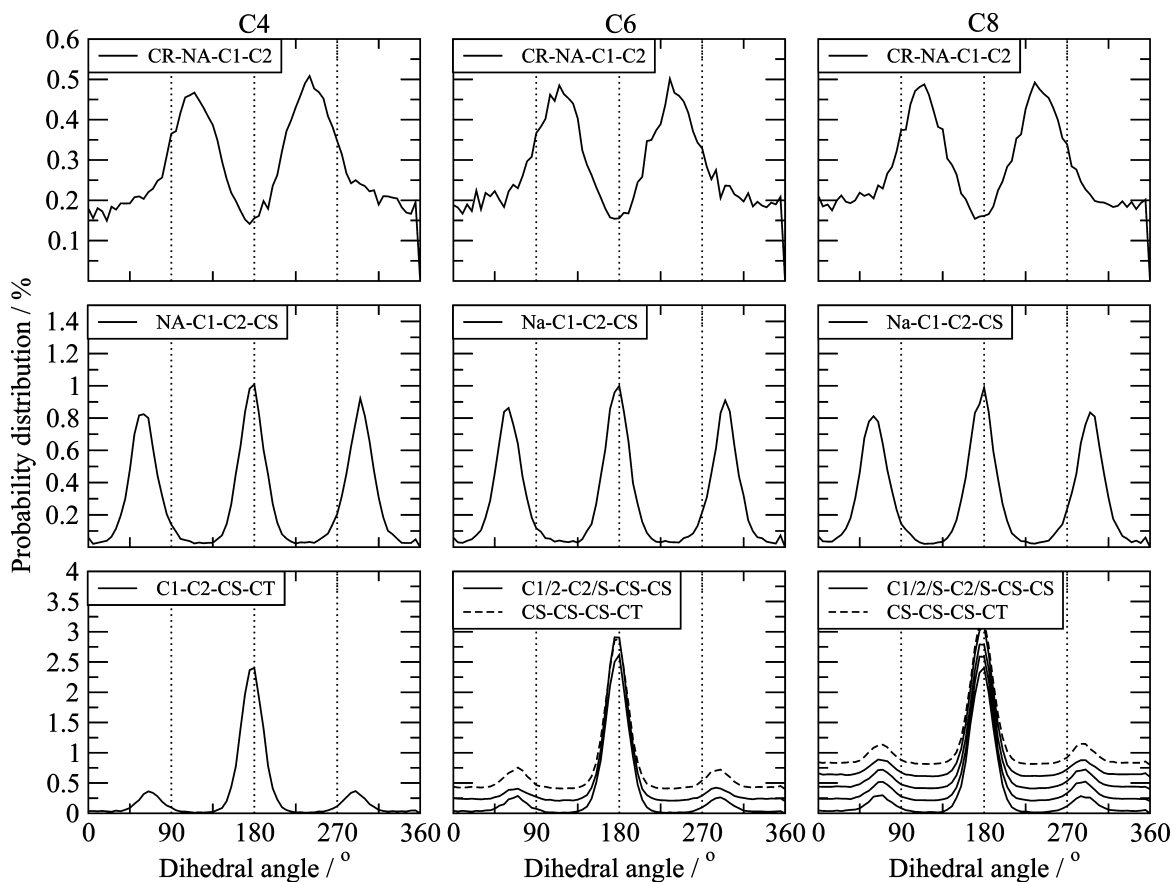
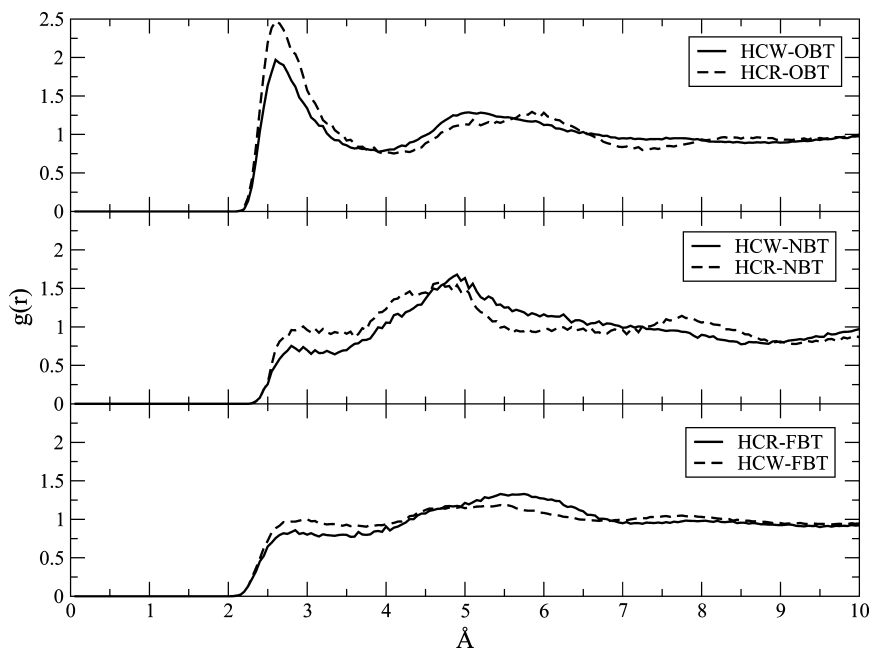


**Figure 11.** Dihedral angles probability distribution for the imidazolium alkyl chain in [C<sub>n</sub>mim][NTf<sub>2</sub>] with  $n = 4, 6,$  or  $8$ . Labeling is defined in Figure 2.

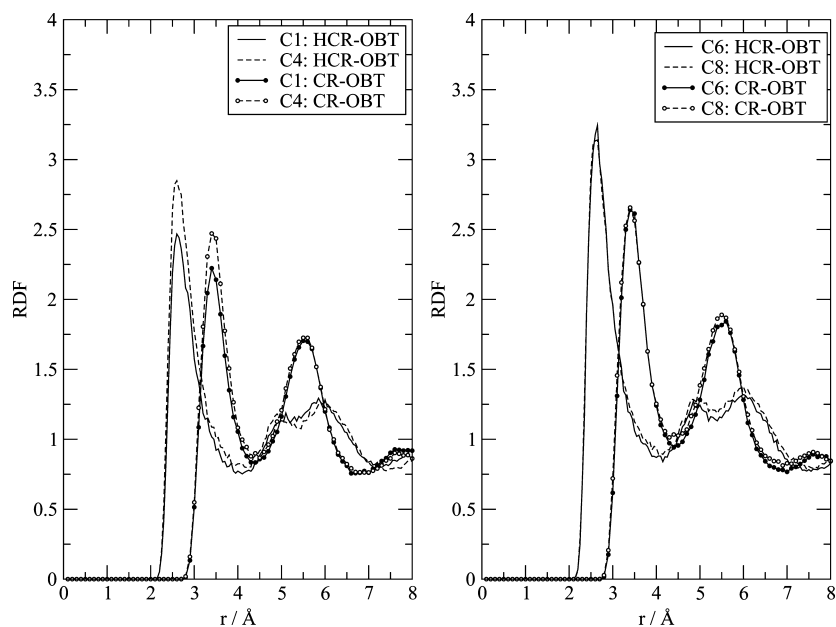
evaluate the average CR–HCR–OBT angle that turns out to be ca. 130°. This means that this kind of hydrogen bonding in these liquids is slightly directional though the H atom lies off the internuclear C–O distance by about 20°.

Figure 14 represents the correlation diagram for the two RDFs for CR–OBT and HCR–OBT for the [C<sub>1</sub>mim][NTf<sub>2</sub>] ionic liquid. Each point of the diagram represents a possible value of the CR–HCR–OBT angle (except those points that do not fulfill the triangular condition such as those in the lower right half of

the square). Three contours are plotted, each enclosing the zone where the angle has the values: 30, 90, and 120°. On top of these regions we have plotted the contours of the angular distribution function obtained as a product of the two RDFs. This distribution shows a sharp peak at the point with coordinates (3.5, 2.5), which means an angle around 120°. This sharp distribution is compatible with a rather directional hydrogen bonding feature between the OBT atom and the CR atom of the imidazolium ring.



**Figure 12.** HCW/HCR RDF with various negatively charged atoms in the  $[C_1mim][NTf_2]$  ionic liquid. Labeling is defined in Figure 2.



**Figure 13.** HCW/HCR–OBT RDF for the  $[C_nmim][NTf_2]$  ionic liquids with  $n = 1, 4, 6,$  or  $8$ .

## Conclusions

Measurements of the X-ray diffraction data for the pure ionic liquids  $[C_nmim][NTf_2]$  with  $n = 1, 4, 6,$  or  $8$ , have been reported for the first time, and interpreted by extracting the corresponding simulated structure factor from all-atom MD calculations. In particular, the current force fields provide a local geometric structure of the pure liquid, which is in very good agreement with the experimental data. Both force fields are able to provide an accurate description of the intramolecular structure and a fairly good description of the intermolecular local structure. In terms of static structure factors, the two force fields do not show substantial differences, and it would be difficult to judge which one scored better in this particular aspect of the simulation.

The simulation confirms once again some of the structural features of these ionic liquids, such as the chain–chain segregation effect on a scale of about  $5\text{--}6$  Å. The geometric conformations of the anion and of the alkyl chains attached to

the imidazolium ring have also been analyzed. In the liquid phase, the anion is found in the preferred trans conformation, and the alkyl side chains are characterized by a sequence of dihedral angles in the anti conformation. The conformation of the side chain is less rigid close to the imidazolium ring, where there is a certain rotational mobility. In  $[C_1mim][NTf_2]$ , a new feature shows up that is due to an intermolecular long-range ordering effect, which is probably allowed by the absence of a lateral chain and involves predominantly the carbon atoms on the ring. A global RDF has been extracted from experimental and simulated data, allowing the interpretation of the main features of the experimental peaks in terms of atomic pair contributions. Even in this case, the two force fields employed here have not shown substantial differences. We have also analyzed the behavior of the hydrogen bonds that are formed between the acidic imidazolium protons and the anion: the electron donors are almost exclusively the oxygen atoms of the

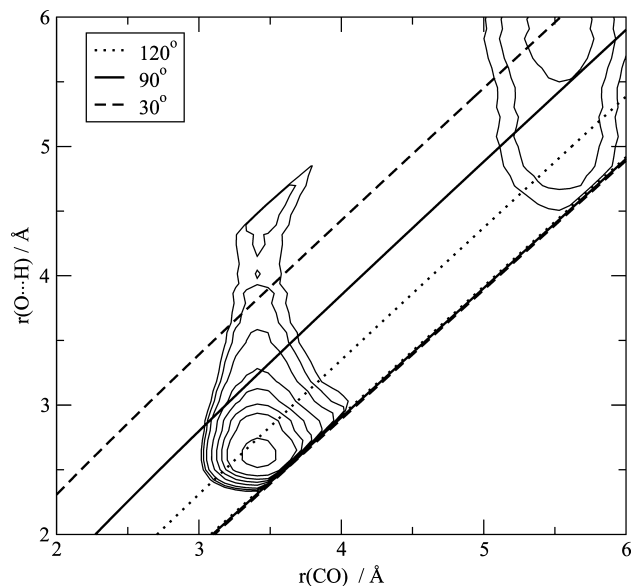


**Figure 14.** Radial correlation plot for the OBT–HCR and CR–OBT distances in the [C<sub>1</sub>mim][NTf<sub>2</sub>] ionic liquid. See text for details.

sulfonyl groups, despite not being the most negatively charged atoms. The hydrogen bonding is found here to be rather directional and stronger with the HCR hydrogen, with this strength increasing, albeit only slightly, with the size of the side chain.

**Acknowledgment.** Financial support of the Scientific Committee of the University of Rome is gratefully acknowledged. Computational support of the CASPUR and CINECA Supercomputing Centers is also acknowledged. A.T. acknowledges support from the FIRB “Futuro in Ricerca” research project (RBF086BOQ\_001, “Structure and dynamics of ionic liquids”). K.R.S. and N.V.P. thank Dr. David Wassell for his input to the manuscript.

## References and Notes

- (1) *Ionic Liquid Synthesis*, 2nd ed.; Welton, T., Wasserscheid, P., Eds.; Wiley VCH: Weinheim, Germany, 2008; p 721.
- (2) Stark, A.; Seddon, K. R. *Ionic Liquids*. In *Kirk-Othmer Encyclopedia of Chemical Technology*, 5th ed.; Seidel, A., Ed.; John Wiley & Sons, Inc.: Hoboken, NJ, U.S.A., 2007; Vol. 26, pp 836–920.
- (3) Freemantle, M. *An Introduction to Ionic Liquids*; RSC Publishing: London, 2009; p 281.
- (4) Plechkova, N. V.; Seddon, K. R. *Chem. Soc. Rev.* **2008**, *37*, 123–150.
- (5) *Ionic Liquids IIIA: Fundamentals, Progress, Challenges, and Opportunities: Properties and Structure*; Rogers, R. D., Seddon, K. R., Eds.; American Chemical Society: Washington, DC, 2005; Vol. 901, p 356.
- (6) *Ionic Liquids IIIB: Fundamentals, Progress, Challenges, and Opportunities: Transformations and Processes*; Rogers, R., Seddon, K., Eds.; American Chemical Society: Washington, DC, 2005; Vol. 902.
- (7) *Ionic Liquids: From Knowledge to Application*; Rogers, R. D., Plechkova, N. V., Seddon, K. R., Eds.; American Chemical Society: Washington, DC, 2009; Vol. 1030, p 464.
- (8) *Molten Salts and Ionic Liquids: Never the Twain?*; Gaune-Escard, M., Seddon, K. R., Eds.; Wiley: New York, NY, U.S.A., 2010; p 441.
- (9) Maginn, E. J. *J. Phys. Chem. B* **2009**, *113*, 373101.
- (10) Lynden-Bell, R. M.; Atamass, N. A.; Vasilyuk, A.; Hanke, C. G. *Mol. Phys.* **2002**, *100*, 3225–3229.
- (11) Canongia Lopes, J. N.; Deschamps, J.; Pádua, A. A. H. *ACS Symp. Ser.* **2005**, *901*, 134–149.
- (12) Canongia Lopes, J. N. A.; Pádua, A. A. H. *J. Phys. Chem. B* **2006**, *110*, 7485–7489.
- (13) Borodin, O. *J. Phys. Chem. B* **2009**, *113*, 11463–11478.
- (14) Bodo, E.; Gontrani, L.; Triolo, A.; Caminiti, R. *J. Phys. Chem. Lett.* **2010**, *1*, 1095–1100.
- (15) Bonhôte, P.; Dias, A. P.; Papageorgiou, N.; Kalyanasundaram, K.; Grätzel, M. *Inorg. Chem.* **1996**, *35*, 1168–1178.
- (16) Marsh, K. N.; Brennecke, J. F.; Chirico, R. D.; Frenkel, M.; Heintz, A.; Magee, J. W.; Peters, C. J.; Rebelo, L. P. N.; Seddon, K. R. *Pure Appl. Chem.* **2009**, *81*, 781.
- (17) Chirico, R. D.; Diky, V.; Magee, J. W.; Frenkel, M.; Marsh, K. N. *Pure Appl. Chem.* **2009**, *81*, 791.
- (18) Lopes, J. N. C.; Deschamps, J.; Pádua, A. A. H. *J. Phys. Chem. B* **2004**, *108*, 2038.
- (19) Dzyuba, S. V.; Bartsch, R. A. *ChemPhysChem* **2002**, *3*, 161–166.
- (20) Fredlake, C. P.; Crosthwaite, J. M.; Hert, D. G.; Aki, S. N. V. K.; Brennecke, J. F. *J. Chem. Eng. Data* **2004**, *49*, 954–964.
- (21) Tokuda, H.; Hayamizu, K.; Ishii, K.; Susan, M. A. B. H.; Watanabe, M. *J. Phys. Chem. B* **2005**, *109*, 6103–6110.
- (22) Jin, H.; O’Hare, B.; Dong, J.; Arzhantsev, S.; Baker, G. A.; Wishart, J. F.; Benesi, A. J.; Maroncelli, M. *J. Phys. Chem. B* **2008**, *112*, 81–92.
- (23) Fujii, K.; Soejima, Y.; Kyoshoin, Y.; Fukuda, S.; Kanzaki, R.; Umebayashi, Y.; Yamaguchi, T.; Ishiguro, S.-i.; Takamuku, T. *J. Phys. Chem. B* **2008**, *112*, 4329–4336.
- (24) Russina, O.; Triolo, A.; Gontrani, L.; Caminiti, R.; Xiao, D.; Hines, L. G., Jr.; Bartsch, R. A.; Quitevis, E. L.; Plechkova, N.; Seddon, K. R. *J. Phys. Condens. Matter* **2009**, *21*, 424121.
- (25) Xiao, D.; Hines, L. G., Jr.; Li, S.; Bartsch, R. A.; Quitevis, E. L.; Russina, O.; Triolo, A. *J. Phys. Chem. B* **2009**, *113*, 6426–6433.
- (26) Tokuda, H.; Hayamizu, K.; Ishii, K.; Susan, M. A. B. H.; Watanabe, M. *J. Phys. Chem. B* **2004**, *108*, 16593–16600.
- (27) Urahata, S. M.; Ribeiro, M. C. C. *J. Chem. Phys.* **2004**, *120*, 1855–1863.
- (28) Wang, Y.; Voth, G. A. *J. Am. Chem. Soc.* **2005**, *127*, 12192–12193.
- (29) Triolo, A.; Russina, O.; Bleif, H.-J.; Cola, E. D. *J. Phys. Chem. B* **2007**, *111*, 4641.
- (30) Triolo, A.; Russina, O.; Fazio, B.; Appetecchi, G. B.; Carewska, M.; Passerini, S. *J. Chem. Phys.* **2009**, *130*, 164521.
- (31) Deetlefs, M.; Hardacre, C.; Nieuwenhuyzen, M.; Pádua, A. A. H.; Sheppard, O.; Soper, A. K. *J. Phys. Chem. B* **2006**, *110*, 12055–12061.
- (32) Canongia Lopes, J. N. A.; Pádua, A. A. H. *J. Phys. Chem. B* **2006**, *110*, 3330–3335.
- (33) Köddermann, T.; Paschek, D.; Ludwig, R. *ChemPhysChem* **2007**, *8*, 2464–2470.
- (34) Köddermann, T.; Paschek, D.; Ludwig, R. *ChemPhysChem* **2008**, *9*, 549–555.
- (35) Logothetis, G.-E.; Ramos, J.; Economou, I. G. *J. Phys. Chem. B* **2009**, *113*, 7211–7224.
- (36) Holbrey, J. D.; Reichert, W. M.; Nieuwenhuyzen, M.; Sheppard, O.; Hardacre, C.; Rogers, R. D. *Chem. Commun.* **2003**, 476.
- (37) Fujii, K.; Fujimori, T.; Takamuku, T.; Kanzaki, R.; Umebayashi, Y.; Ishiguro, S. I. *J. Phys. Chem. B* **2006**, *110*, 8179–8183.
- (38) Lassegues, J. C.; Grondin, J.; Holomb, R.; Johansson, P. J. *Raman Spectrosc.* **2007**, *38*, 551.
- (39) <http://www.iolitec.de>.
- (40) Caminiti, R.; Sadun, C.; Rossi, V.; Cilloco, F.; Felici, R. Italian Pat. Appl. No. 01261484, 1993.
- (41) Gontrani, L.; Russina, O.; Marincola, F. C.; Caminiti, R. *J. Chem. Phys.* **2009**, *131*, 244503.
- (42) Murata, Y.; Nishikawa, K. *Bull. Chem. Soc. Jpn.* **1978**, *51*, 411–418.
- (43) Cromer, D.; Waber, J. Atomic Scattering Factors for X-Rays. In *International Tables for X-Ray Crystallography*; Kynoch Press: Birmingham, U.K., 1974; Vol. 4, pp 71–147.
- (44) Dietrich, H. *J. Appl. Crystallogr.* **1976**, *9*, 238–239.
- (45) Nishikawa, K.; Iijima, T. *Bull. Chem. Soc. Jpn.* **1984**, *57*, 1750–1759.
- (46) Fritsch, G.; Wagner, C. N. *J. Z. Phys. B: Condens. Matter* **1986**, *62*, 189–194.
- (47) Smith; Forester, T. R. *DL POLY, a package of molecular simulation routines*; The Council for the Central Laboratory of the Research Councils, Daresbury Laboratory at Daresbury, North Warrington, U.K., 1996.
- (48) Canongia Lopes, J. N.; Pádua, A. A. H. *J. Phys. Chem. B* **2004**, *108*, 16893–16898.
- (49) Wieder, T.; Füss, H. Z.; Naturforsch., A. *Phys. Sci.* **1997**, *52*, 386–392.
- (50) Gilli, G.; Gilli, P. *The Nature of the Hydrogen Bond: Outline of a Comprehensive Hydrogen Bond Theory*, 1st ed.; International Union of Crystallography Monographs on Crystallography; Oxford University Press: Oxford, U.K., 2009; p 336.
- (51) Kemper, V.; Kirchner, B. *J. Mol. Struct.* **2010**, *972*, 22–34.
- (52) Thar, J.; Brehm, M.; Seitsonen, A. P.; Kirchner, B. *J. Phys. Chem. B* **2009**, *113*, 15129–15132.